IEEE Transactions on Quantum Engineering

Received 22 December 2021; revised 13 August 2022; accepted 8 September 2022; date of publication 19 September 2022; date of current version 13 October 2022.

Digital Object Identifier 10.1109/TQE.2022.3207901

Mode-Manipulated Multimode Cavity for Quantum Memory

TAE HWAN JANG[1,4], JAEHYEONG LEE[1], JAEHO SHIN[1], JINHYOUN KANG[1], SUNGHO HAN[1], INSU JEON[1], SRIVATSAN CHAKRAM[2], DAVID I. SCHUSTER[3], AND HYEOKSHIN KWON[1]

[1]Samsung Advanced Institute of Technology, Suwon-si 16678, South Korea
[2]Department of Physics, Rutgers University, Piscataway, NJ 07102 USA
[3]Department of Physics, University of Chicago, Chicago, IL 60637 USA
[4]School of Electrical Engineering, Hanyang University, Ansan 15588, South Korea

Corresponding authors: Jaeho Shin and Hyeokshin Kwon (e-mail: jaehho.shin@samsung.com; hs78.kwon@samsung.com).

ABSTRACT In this article, a quasi-elliptical geometry and the iris technique are applied to a multimode cavity to manipulate the resonant mode in the desired direction for quantum memories. By applying quasi-elliptical geometry, the characteristics of monotonically increasing, equally spaced, and monotonically decreasing frequency intervals between the modes are realized. To manipulate a certain mode, an iris is applied to the multimode storage cavity. As an example, the entire mode, including the readout cavity, is implemented at equal intervals to minimize the interference and maximize the mode number from adjacent modes for the 5–8 GHz frequency band.

INDEX TERMS Cavity, frequency spectrum, iris, multimode cavity, quantum memory.

I. INTRODUCTION

With the rise of technological domains such as cryptography [1], machine learning [2], computational chemistry [3], and database searching [4], which require processing massive amounts of data or information, the need for new, more efficient computing methods that go beyond the capabilities of existing computers is being felt. In this respect, quantum computing is rapidly emerging as promising research topic.

One way to implement quantum computing is to use quantum memory (QM). Fig. 1 shows a conceptual diagram of a multimode QM. As shown in the figure, a qubit is simultaneously coupled to several multimode storage and readout modes. Because the multimode cavity is simultaneously coupled and controlled by a physical qubit, this could be an efficient way to construct QMs. This method also has an additional advantage in that it is ideal for reducing physical lines while realizing multiqubit QMs, which is helpful in dealing with complexity. The detailed process of conducting quantum operations is described in [5], [6], and [7].

Various types of research have been conducted on QM [8], [9], [10], [11], [12], [13], [14], [15]. In these studies, QMs were implemented using coplanar waveguide line resonators coupled with a superconducting qubit in an on-chip structure [8], [9] or 3-D cavity resonator [10], [11], [12], [13], [14], [15]. Generally, the on-chip method occupies a smaller volume than the 3-D cavity method but achieves a lower Q-factor compared with the 3-D cavity. The Q-factor is an important parameter that affects the coherence time of QMs. In this article, a 3-D cavity-based method was chosen because of its high Q-factor.

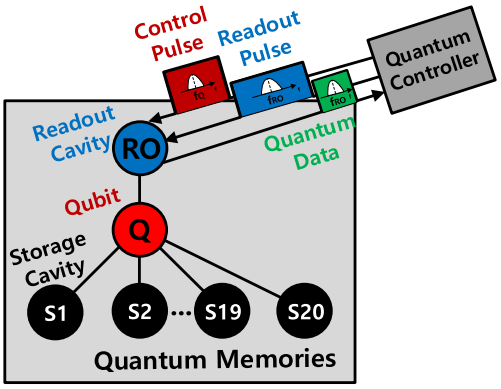

FIGURE 1. Conceptual diagram of multimode quantum memories.

It has also been reported that applying multiple storage resonators is advantageous over using a single resonator in terms of qubit connectivity by implementing random-access control [10], [14], [15], [16], [17], [18].

This work is licensed under a Creative Commons Attribution 4.0 License. For more information, see http://creativecommons.org/licenses/by/4.0/

Implementing a QM using a cavity involves storing, calculating, and reading quantum information by using photon Fock states of $|0\rangle$ and $|1\rangle$ as qubits through interactions and coupling with transmon qubits. Methods for realizing QMs include sidebands [15], blue sidebands [16], selective number-dependent arbitrary phase gates [17], and photon blockades [18].

Fig. 2 shows a conceptual diagram of the frequency spectrum of a multimode QM. To realize QMs, the overall resonant frequencies of the component constituting the QMs should be placed with a spacing of at least Δ, considering the qubit-cavity coupling, signal bandwidth, thermal noise, and other interference. Δ is the available bandwidth per storage mode. In this article, the available bandwidth was set to 3 GHz, and the number of storage modes was 20; therefore, Δ corresponds to 150 MHz.

It is need to consider that the readout is placed as far as possible from the qubit frequency because the qubit should not be affected when performing the measurement. Therefore, the resonant frequencies of the storage cavity were placed between the qubit and readout frequencies.

Moreover, unlike rectangular readout signals, Gaussian pulses are generally used for qubit excitation owing to the narrow bandwidth of Gaussian signals. However, to implement such a signal, a digital-to-analog converter (DAC) with an extremely high sampling rate versus frequency is required. Therefore, the qubit frequency was selected to be lower than the frequency of the storage mode in order to reduce the required sampling rate of the DAC in the case of direct digital synthesis.

In addition, because the transmon itself is very fine and the fabrication error is large compared with the readout cavity, it is relatively difficult to realize the qubit frequency between the desired storage cavity mode frequencies. Therefore, the qubit frequency was selected to be lower than the frequency of the storage mode rather than the readout mode frequency.

If each resonant frequency is randomly placed, it can be clearly shown that only a few resonant frequencies can be placed between the given bandwidth and readout frequency.

Although it is impossible to place the frequencies equally spaced because each resonant frequency of a storage cavity has a dependent relationship, it is possible to arrange the resonant frequency of the storage cavity close to equal intervals using a parabolic-shaped cavity [18], [19], [20]. Nevertheless, the structure can be modified to enable an equally spaced arrangement of the resonant frequency of the storage cavity rather than a parabolic-shaped cavity.

If the number of memory modes is increased at equal intervals, the specific memory mode and readout mode may overlap. Just as qubits are coupled with the readout, they are coupled with the memory modes. Therefore, when a pulse is applied to the qubit, the frequency of the readout and memory modes changes.

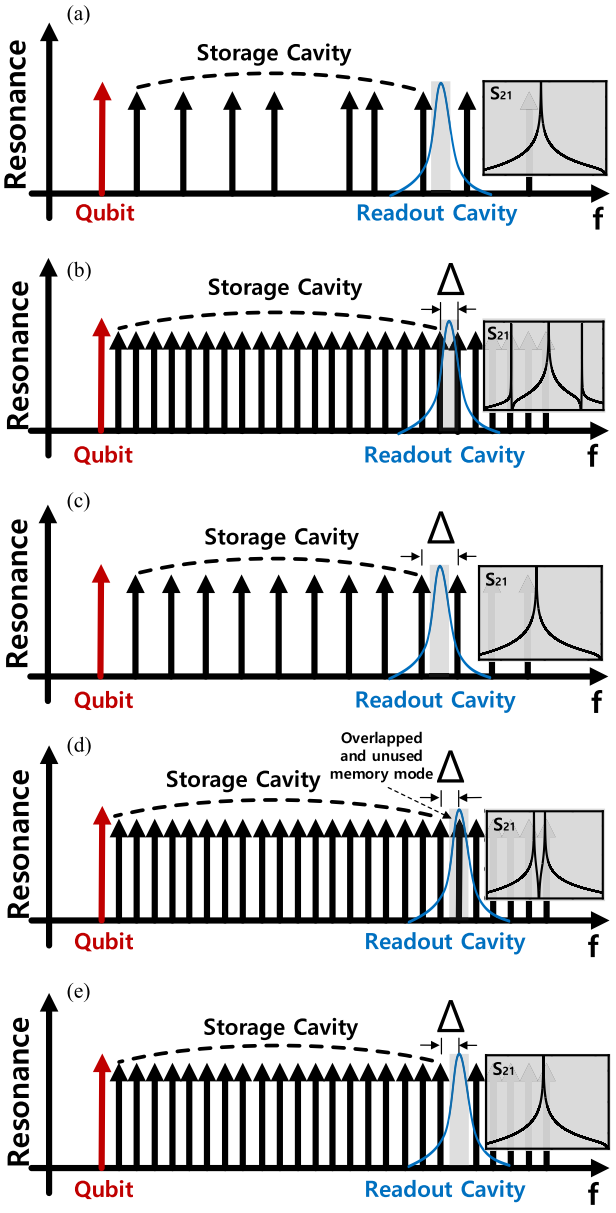

FIGURE 2. Conceptual diagram of the frequency spectrum for multimode quantum memories. (a) Case in which the resonant frequencies of the components are randomly separated. (b) Case in which only the resonant frequencies of the storage cavity are equally spaced. (c) Case in which only the resonant frequencies of the storage space are evenly spaced apart, and the resonant frequency interval between the readout frequency and storage frequency is double compared with Fig. 2(b). (d) Case in which the storage mode that overlaps with the readout frequency is left unused. (e) Case in which overall resonant frequencies of the quantum memories are equally spaced, with a missing mode at the frequency of the readout cavity.

When using the memory mode adjacent to the readout frequency, placing a pulse in the memory mode will affect the readout frequency, which will also affect the qubits [see Fig. 2(b)]. In other cases, it is assumed that only the readout frequency and distant memory modes are used, leaving an overlap between the readout frequency and memory modes.

IEEE Transactions on Quantum Engineering

For the measurement, the readout frequency must be applied [see Fig. 2(d)]. Then, photons are activated in the memory modes adjacent to the readout frequency, and qubits are affected by these activated memory modes.

In summary, memory mode is turn ON and OFF only when used, but because the qubit and coupling exist even in the off state, the fidelity of the system can be increased by removing the memory modes adjacent to the readout frequency. To reduce the OFF-resonant interactions, a mode spacing of 200–250 MHz was chosen in [19].

To solve this issue, the following case is considered. The nth resonant frequencies were shifted to where the $(n+1)$th resonant frequencies were originally, and the readout frequency was shifted to where the nth resonant frequencies were originally.

It is obvious that the overall resonant frequencies of QM devices are equally spaced with an interval greater than Δ, so that the maximum number of modes can be created in a given bandwidth.

In this article, by applying a quasi-elliptical geometry, it was possible to make the distance between the modes of the storage cavity equidistant. Furthermore, by placing the iris structure inside the storage cavity, it was shown that each resonance frequency of the multimode cavity could be manipulated into the desired form. As an example, it was proposed that the entire mode, including the readout cavity, be implemented at equal intervals to maximize the resonant modes and minimize the interference from adjacent modes in a given bandwidth.

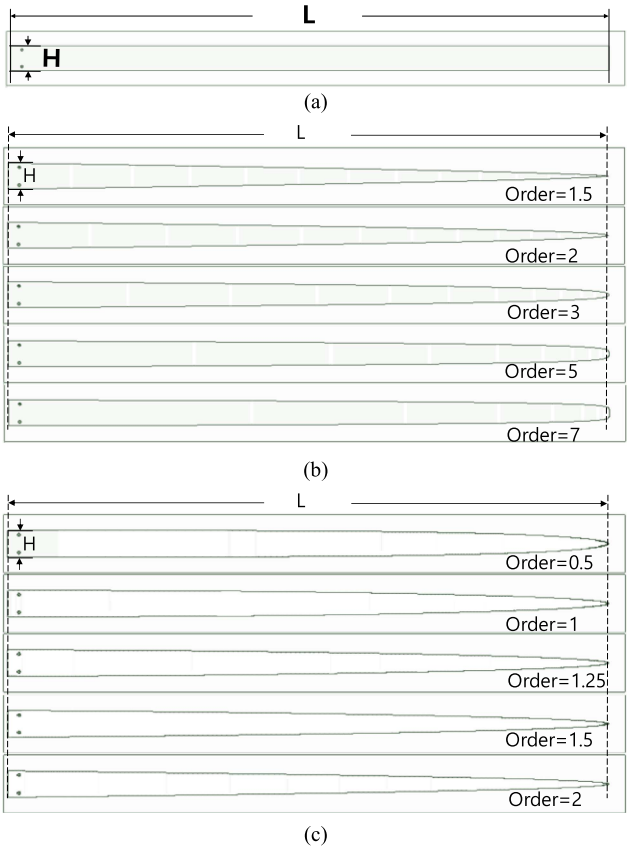

FIGURE 3. Geometry of the cavity when applying various geometries. (a) Rectangular case. (b) Parabolic case. (c) Quasi-elliptical case.

II. STORAGE CAVITY DESIGN

A. CAVITY GEOMETRY DESIGN

To realize a QM for 3-D cavity-based multimode QM, a multimode storage cavity must be designed. Fig. 3 shows the cavity geometry for various geometries. Generally, the mode frequencies of a rectangular multimode cavity are represented by the following equation:

$$f_{l,m,n} = \frac{c}{2\pi}\sqrt{\left(\frac{l\pi}{H}\right)^2 + \left(\frac{m\pi}{W}\right)^2 + \left(\frac{n\pi}{L}\right)^2} \tag{1}$$

where W, L, and H are the width, length, and height, respectively, of the rectangular cavity. For L>H>>W and m = 1, the equation can be expanded as follows:

$$f_{10,n} \sim \frac{c}{2H} + \frac{cH}{4L^2}n^2. \tag{2}$$

From this equation, it can be seen that the interval between modes gradually increases as the mode number increases; therefore, the geometry of the cavity needs to be revised.

In [18], [19], and [20], it was realized that the effective length of a cavity increases in proportion to $\sqrt{n}$ ($L_{eff} \sim k\sqrt{n}$, where k is a proportional constant, and that the resonant frequency increases by equal intervals when the mode number is increased. The interval between each mode was calculated as follows:

$$f_{10,n} - f_{10,(n-1)} \sim \frac{cH}{4k}. \tag{3}$$

In the case of a parabolic geometry, the effective length does not increase in proportion to $\sqrt{n}$ on the order of two. Because, it is difficult to realize precise equidistant intervals for adjacent modes when designing a cavity using parabolic geometry on the order of 2; in this article, quasi-elliptical geometry is applied to precisely implement equidistant characteristics.

Cavities using parabolic and quasi-elliptical geometries were designed using

$$a\left(\left(\frac{2}{H}t\right)^{\alpha} - 1\right) = x,\ t = z \tag{4}$$

$$x = L\sin(t)^{\alpha},$$

$$z = \frac{H}{2}\cos(t)\ (0 < t < \pi) \tag{5}$$

where a, L, and H are selected as 0.6, 600, and 26 mm, respectively. Fig. 4 shows the frequency interval between adjacent modes when various geometries are applied.

In the case of a rectangular cavity, the frequency interval increased from 0.0162–0.1661 MHz as the mode number

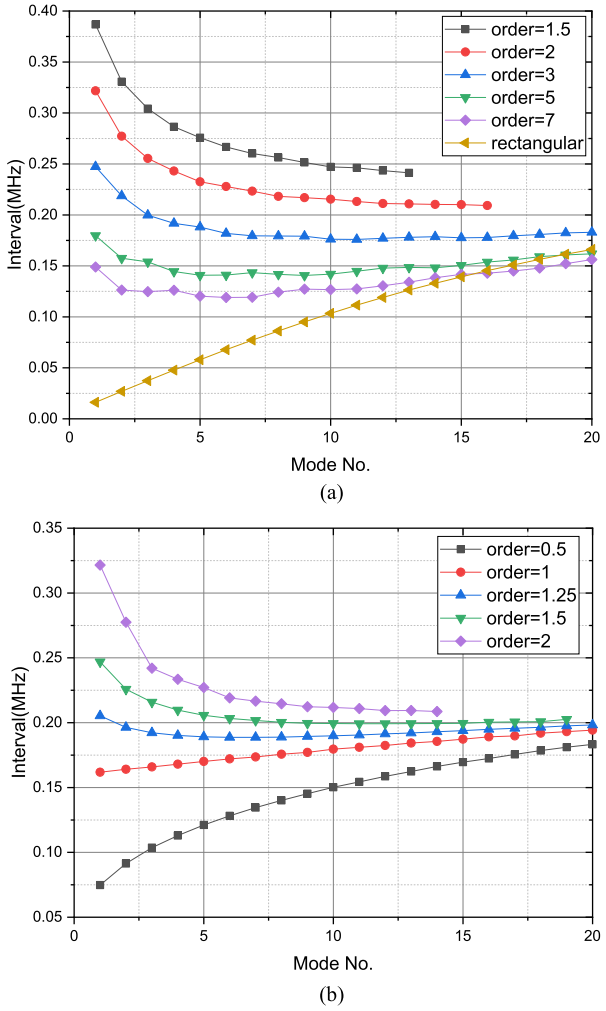

FIGURE 4. Frequency interval between adjacent modes when applying various geometries. (a) Rectangular and parabolic case. (b) Quasi-elliptical case. The first mode frequency is fixed to approximately 5 GHz.

increased from 1–21. Because the ratio of the first interval to the last interval is 10.25 (= 925% difference), most frequencies are distributed in the low-frequency region in a rectangular cavity. Therefore, it is difficult to use it as an actual multimode QM.

If the parabolic geometry is applied for a multimode cavity with order of 2, the frequency interval is decreased from 0.3217–0.2092 MHz as the mode number increases from 1–16, and the ratio of the interval corresponds to 1.53 (= 53% difference). If a parabolic geometry is applied to a multimode cavity on the order of five, the frequency interval remains almost stable. The interval with the largest difference is 0.1797 MHz in the first mode, the interval with the smallest difference is 0.1406 MHz in the 9th mode, and the ratio of the interval corresponds to 1.278 (= 27.8% difference). If quasi-elliptical geometry is applied on the order of 1.25, the frequency interval remains almost stable. The interval with the largest difference was 0.2053 MHz in the first mode, the interval with the smallest difference was 0.1887 MHz in the 6th mode, and the ratio of the interval corresponded to 1.086 (8.6% difference).

From This result, it is clear that it is advantageous to use an elliptical cavity to realize equally spaced resonant frequencies.

Moreover, the use of quasi-elliptical geometry has several advantages.

1) It is possible to implement all the characteristics of the frequency intervals, including monotonically increasing, equal spacing, and monotonically decreasing, without significant changes in the order.
2) In contrast to the parabolic case, it is possible to implement monotonically increasing frequency interval characteristics.
3) In addition, in contrast to the parabolic case, it is advantageous to optimize the interval characteristics because the high-order mode frequency interval does not change even after an order sweep.

Thus, in this article, a quasi-elliptical geometry was applied in the multimode cavity design.

TABLE 1. Dimension of the Proposed Multimode Storage Cavity

Parameter	Value (mm)	Parameter	Value (mm)
H_c	29.7	H_T	60.1
D_C	6	D_I	4
L_C	568	L_{offset}	250
$P_{iris,1}$	13.2	$P_{iris,2}$	37.4
$P_{iris,3}$	61.6	$P_{iris,4}$	84.7
$P_{iris,5}$	108.9	$P_{iris,6}$	133.1
$P_{iris,7}$	156.2	$P_{iris,8}$	181.5
$P_{iris,9}$	206.8	$P_{iris,10}$	231
$P_{iris,11}$	255.2	$P_{iris,12}$	280.5
$P_{iris,13}$	306.9	$P_{iris,14}$	331.1
$P_{iris,15}$	357.5	$P_{iris,16}$	385
$P_{iris,17}$	413.6	$P_{iris,18}$	442.2
$P_{iris,19}$	471.9	$P_{iris,20}$	504.9
$P_{iris,21}$	541.2	D_G	2.9
α	1.25	D_{IG}	3.2

* H_c: Height of inner cavity, H_T: Total height of cavity, D_C: Diameter of hole, D_I: Diameter of iris, L_C: Total length of cavity, L_{offset}: Original length of the quasi ellipse - L_C, $P_{iris,n}$: The length from the starting point to the center of the n^{th} iris, D_G: gap between the center of the hole to center of the adjacent hole, and D_{GI}: gap between the center of the hole to center of the iris.

B. IRIS-BASED SPECIFIC MODE MANIPULATED MULTIMODE STORAGE CAVITY

As shown in Fig. 5(a), a multimode cavity is designed with a quasi-elliptical geometry to form the maximum number of resonant frequencies in a given bandwidth. Table 1 shows the dimensions of the proposed multimode storage cavity.

A perfect electric conductor was assigned to the cavity to assume a superconductivity condition, and this cavity was simulated using the full-wave EM solver HFSS. This cavity was fed by two input and output ports, and the strength of the

IEEE Transactions on Quantum Engineering

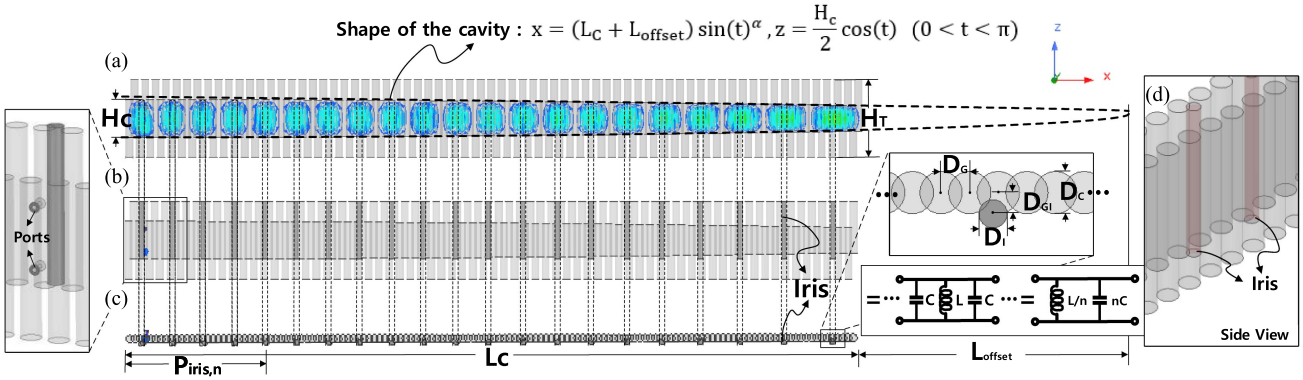

FIGURE 5. Geometry and field distribution of the multimode storage cavity. (a) 21st mode of the multimode storage cavity without iris at 7.8646 GHz. The multimode cavity with quasi-elliptical geometry, and quasi-elliptical multimode cavity with iris in (b) front view, (c) top view, and (d) 3-D perspective view.

transmission coefficient and external Q-factor was controlled by sweeping the signal pin length of each port.

In this article, a quasi-elliptical geometry for multimode cavities was realized using this equation

$$x = (L_c + L_{offset})\sin(t)^{\alpha},\ z = \frac{H_c}{2}\cos(t)\ (0 < t < \pi)\ . \tag{6}$$

This cavity is also designed in a flute-shape to realize a seamless function and obtain a high Q-factor, as explained in detail in [18], [19], and [20]. A conventional cavity was created by connecting two cavities. However, the seam, which is a mismatch between the connected boundaries, causes a decrease in the Q-factor. A flute-shaped cavity was fabricated by drilling holes alternately up and down, and the overlapping part was used as the cavity. The diameter of the holes is much smaller than the wavelengths of the target frequencies ($D_c << \lambda$); therefore, most of the electromagnetic field is trapped in the cavity without escaping through the hole. Furthermore, a Q-factor much higher than 10^9 is revealed, such that the quantum information is almost unaffected by the external environment.

To arrange all the resonant frequencies constituting the QMs for multimode QMs equally, the resonant frequency of the storage cavity corresponding to the potential readout frequency should be moved upward by the frequency interval, so that the readout frequency can be placed at the location at which the shifted resonant frequency of the storage cavity was originally placed.

Fig. 5(b) and (c) shows a multimode cavity with irises. An iris, which is the ridge shape inside a cavity, a conducting plate fitted transversally across the waveguide with a large aperture, was used to implement a filter to cut off unnecessary frequency bands, as in [21], [22], [23], [24], [25], and [26], which is known as a ridged structure [27]. In this article, an iris, which is created by drilling an additional hole drilled OFF-center to the existing storage cavity was used to control the specific mode of the cavity resonator to realize QMs with maximized modes.

Moreover, to shift the target mode frequencies, irises must be placed at each center of the point at which the strength of a mode is maximized to prevent the formation of a resonant mode at the target frequency. In this article, 21 irises were inserted at the locations along the cavity where the field antinodes of the 21st mode would occur in the absence of irises.

From the field distribution of the 21st mode, it is clear that a field is not formed except around the ports if irises are inserted into the multimode cavity. Therefore, it can be concluded that the irises interfere with mode formation at a specific frequency such that a specific frequency is shifted to a nearby frequency.

According to [27], the periodic arrangement of an iris can be easily approximated using an *LC* circuit (the gap between the ridges is represented by capacitance *C*, and each side section of the ridged waveguide can be represented by inductance). From Fig. 5, the cavity can be analyzed by an *LC* array, and this is summarized as the inductance of L/n and capacitance nC, where n is the number of irises. Therefore, the cutoff frequency that does not allow any wave to pass through can be approximately calculated using the following equation, and this formula is independent of the number of irises:

$$f_c \sim \frac{1}{2\pi\sqrt{LC}} = \frac{1}{2a\sqrt{\mu_0\epsilon_0}}\left[\frac{2}{\pi}\sqrt{\left(\frac{a}{a_0}\right)\left(\frac{b_0}{b}\right)\left(\frac{1}{1-\frac{a_0}{a}}\right)}\right] \tag{7}$$

where $a = L_C/21, a_0 = a - D_I, b = \frac{1}{2}D_C + \frac{1}{2}D_I + D_{IG}$, and $b_0 = D_C$.

By applying the value in Table 1, f_c value was calculated as being 8.4 GHz.

Fig. 6 shows the effective length of a multimode cavity with a quasi-elliptical geometry along the mode numbers. The effective length of a cavity is defined in the manuscript as the length at which a field with an intensity of 1/10 of the maximum field can exist in the cavity. Because the cavity has a quasi-elliptical shape, a lower effective length is obtained by lowering the frequency, which corresponds to a low

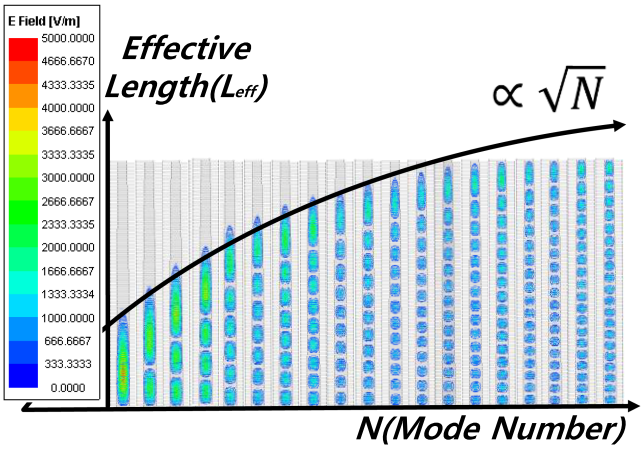

FIGURE 6. Effective length of the multimode cavity with quasi-elliptical geometry along the mode numbers.

mode number because the electromagnetic field cannot pass through an area lower than a certain height. Therefore, it is clear that the effective length of the cavity is proportional to $\sqrt{n}$.

Fig. 7 shows the simulated transmission coefficient of a quasi-elliptical multimode cavity with and without an iris. If the irises are placed in the field of the antinodes of the 21st mode, the gap between the 20th and 21st modes widens the existing spacing by approximately two times. This was because the iris was inserted to prevent any mode from occurring at the frequency corresponding to the 21st mode of the existing cavity.

In the case of a quasi-elliptical cavity without irises, the interval between the first mode and the second mode was 143 MHz, and the interval between the 20th and 21st modes was 157 MHz. In this case, if the resonance mode of the readout cavity is inserted between the 20th and 21st modes of the storage cavity, the frequency difference between the memory cavity and readout can be maximized up to 157 MHz. Because the spacings of all modes are not equal, this is inefficient in terms of frequency utilization.

If the irises are equally spaced, because they shift not only the target mode frequency but also the adjacent mode frequencies, the intended characteristics cannot be expected. Although the readout frequency was between the 20th and 21st modes, the entire mode could not be arranged at equal intervals.

It is shown that the interval between the first mode and the second mode is 133 MHz, and the interval between the 20th and 21st modes is 270 MHz, and hence, the modes are maximally utilized in a given bandwidth when the irises are placed at the field antinodes of the 21st mode.

Fig. 8 shows the E-field distribution of a multimode storage cavity with and without an iris structure. If an iris is added, then a shunt capacitor is added to the desired local area in the cavity to change the impedance at the desired point. The input impedance was originally infinite at the

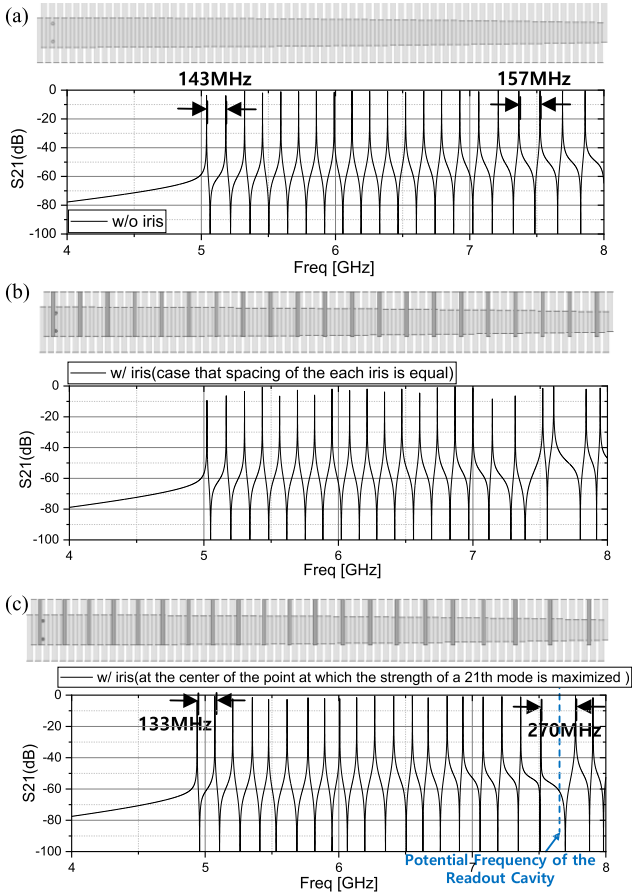

FIGURE 7. Simulated transmission coefficient of the quasi-elliptical multimode cavity (a) without irises, (b) with equally-spaced irises, and (c) with irises placed at the positions of the field antinodes of the 21st mode.

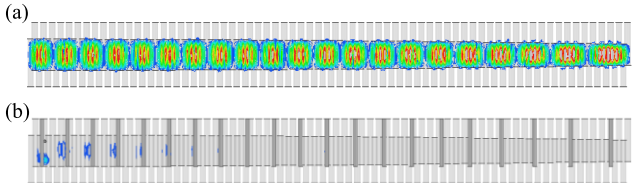

FIGURE 8. E-field distribution of the 21st mode of the multimode storage cavity with and without iris structure at 7.8646 GHz. (a) Without irises. (b) With irises.

point where the intensity of the existing mode was maximized. When adding irises to the points at the field antinodes of the mode, a parallel capacitor was added to lower the impedance, and the mode was not formed at the desired frequency. It was confirmed that only a few fields were formed by placing the irises at the field antinodes of the 21st mode. In addition, adjacent modes (21st and 20th modes) of the corresponding frequency were formed at a point away from the corresponding frequency.

Fig. 9 shows the simulated transmission coefficient of the quasi-elliptical multimode cavity with the irises obtained by

IEEE Transactions on Quantum Engineering

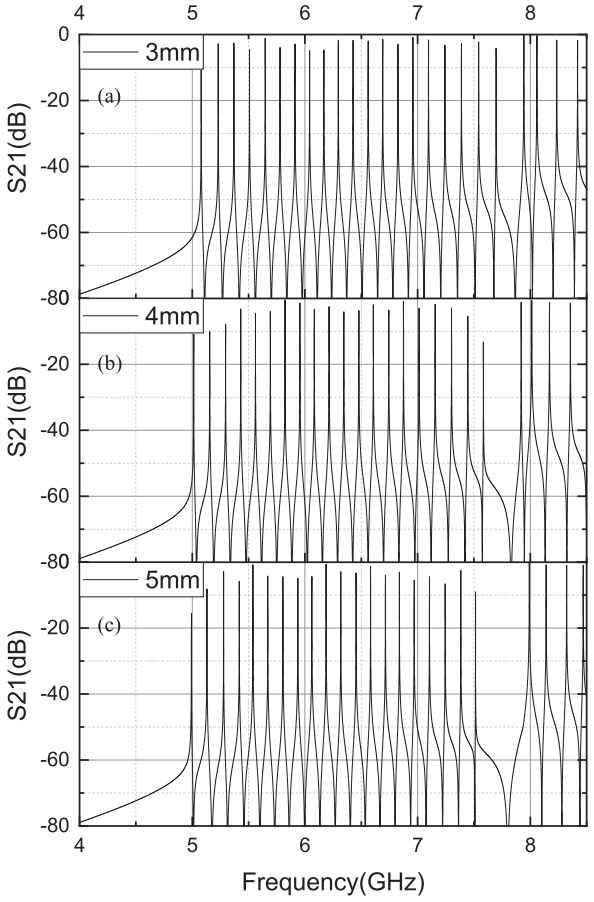

FIGURE 9. Simulated transmission coefficient of the quasi-elliptical multimode cavity with irises by sweeping DI. (a) 3 mm case. (b) 4 mm case. (c) 5 mm case.

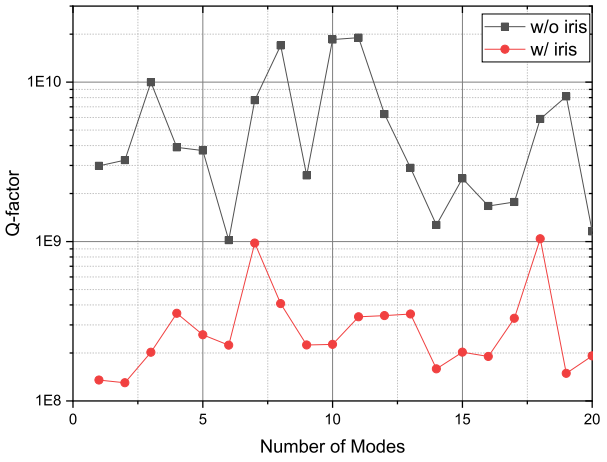

FIGURE 10. Simulated internal Q-factor of the quasi-elliptical multimode cavity with and without irises.

sweeping D_I. It is shown that the cutoff frequency value is observed around 7.8 GHz. The difference between the calculated and simulated values was approximately 0.6 GHz.

This error occurred because (7) should have been applied to the rectangular cavity, but was applied to the elliptical cavity with a flute-shaped structure.

In the simulation, the transmission coefficient was observed by tuning the iris diameter. The gap between the 20th and 21st modes increases as the D_I increases.

This is because, as D_i increases, the ratio of the iris to the entire cavity structure increases; thus, the bandwidth that generates any mode near the 21st frequency gradually increases. Therefore, the bandwidth near the 21st frequency, which prevents the occurrence of any resonance frequency, is widened by increasing D_i. QM design with maximized modes for 3-D cavities based on multimode QM is possible by tuning the radius of the iris to form a gap between the 20th and 21st modes, which is twice the required minimum spacing of the mode. Fig. 10 shows the simulated internal Q-factor of the quasi-elliptical multimode cavity with and without the irises. In the simulation, the conductivity of the cavity was set to 10^{30}S/m considering that the cavity was in a superconducting state. The Q-factor tends to deteriorate by approximately 10 times because the field leaks more than that of a cavity without an iris. Considering that T_1 and T_2 were measured at approximately 2 ms when experimenting with a resonator with a Q-factor of less than 10^8 [19], it is expected that T_1 and T_2 can be achieved at least higher than 2 ms. In addition, it is possible to further improve the Q-factor if the size of the hole constituting the iris is small.

Fig. 11 shows the simulated transmission coefficient of the quasi-elliptical multimode cavity with the iris obtained by sweeping the mode number. It was confirmed that the desired mode could be controlled by placing the field antinodes of each mode.

Fig. 12 shows the geometry of the curved multimode storage cavity. To conduct a quantum operation, QMs are embedded in a dilution refrigerator, which maintains a temperature of up to 10 mK to minimize thermal noise and prevent thermal excitation of the qubit. However, because the length of the entire multimode cavity is too long to be embedded in the fridge, the length of the cavity should be reduced. Therefore, the shape of the multimode should be transformed into a meandered shape to reduce the length and transform the shape of the cavity into a form that fits the fridge. This cavity is also intended to place 20 modes in the given frequency band (5–8 GHz), and by placing the iris at the field antinode of the 21st mode, it is designed for QM with maximized modes as well. The curved multimode storage occupies a volume of $46 \times 200 \times 60$ mm^3.

Fig. 13 shows the fabricated flute-shaped multimode cavity resonator. The cavity was designed using aluminum. Fig. 14 shows the simulated and measured transmission coefficients of the proposed flute-shaped multimode cavity resonator. Because the cavity was measured at room temperature, the transmission coefficient was as low as 20 dB because the total Q-factor decreased owing to deterioration in the internal Q-factor. Compared with the simulated results, the measured results show downshifted resonant frequencies as

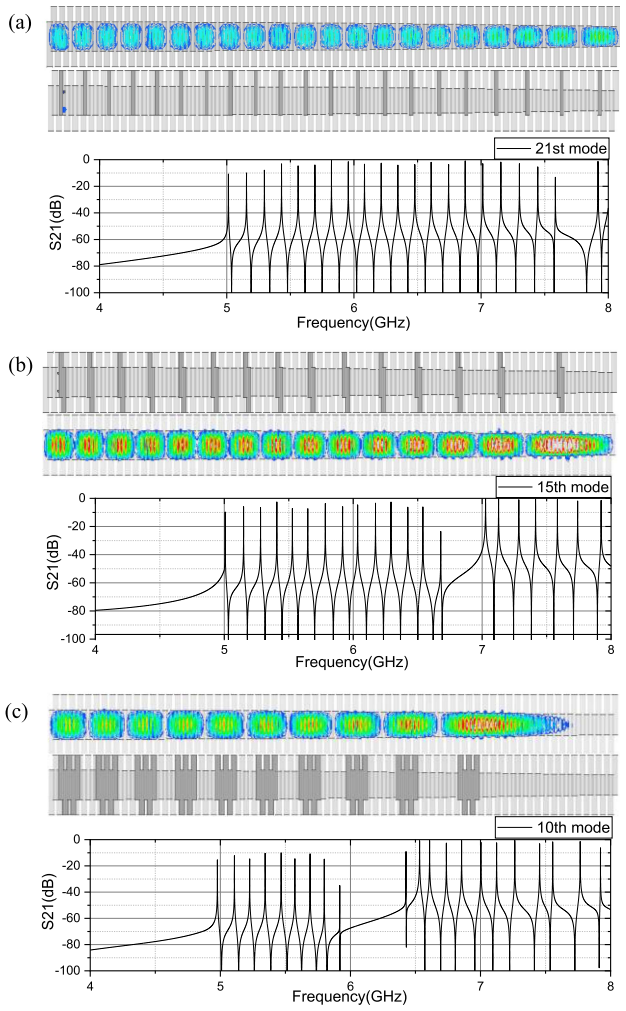

FIGURE 11. Simulated transmission coefficient of the quasi-elliptical multimode cavity with irises by sweeping mode number. The magnitude of the E-field is displayed on a color scale. (a) 21st mode, (b) 15th mode, and (c) 10th mode.

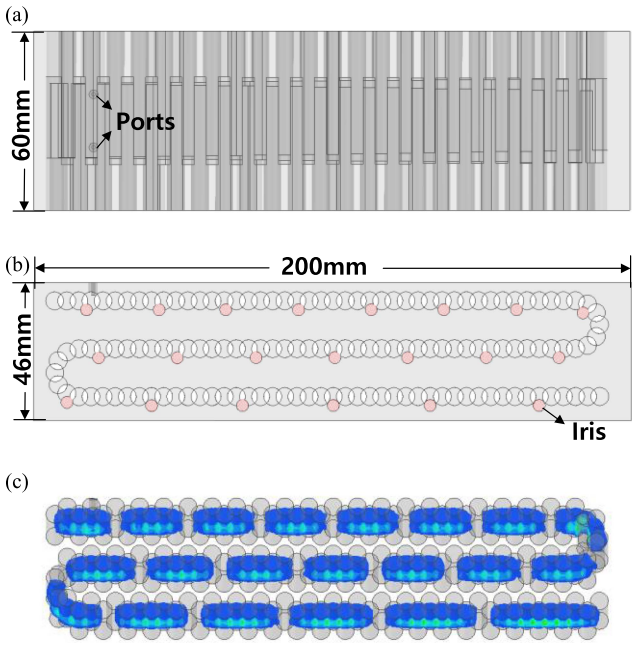

FIGURE 12. Geometry of the curved multimode storage cavity. (a) Side view of multimode cavity with irises. (b) Top view of multimode cavity with irises. (c) Field distribution of multimode storage cavity without irises.

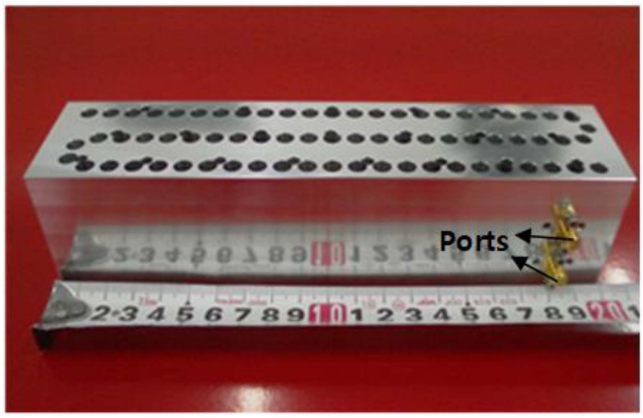

FIGURE 13. Fabricated proposed flute-shaped multimode cavity resonator. The unit spacing of the ruler is given in cm.

low as 30 MHz. The shift is caused by a fabrication error, and considering the first resonant frequency of 5 GHz, a 30 MHz shift is only 0.6%.

III. QUANTUM MEMORIES WITH MAXIMIZED MODES USING PROPOSED SPECIFIC MODE MANIPULATED MULTIMODE CAVITY

In this article, it was proposed that the entire mode, including the readout cavity, be implemented at equal intervals to maximize the resonant modes and minimize the interference from adjacent modes in a given bandwidth as an example for multimode QMs.

Fig. 15 shows a QM with maximized modes using the proposed specific mode-manipulated multimode storage cavity. A QM with maximized modes is designed such that all resonance modes, including the readout mode, are equally spaced by placing the readout frequency between the 20th and 21st resonance frequencies of the storage resonator.

A QM with maximized modes consists of a storage cavity that stores quantum information, a qubit that performs quantum operations, and a readout cavity that reads the performed quantum computation. The cavity is modeled as a perfect electric conductor because it exhibits superconductivity at 10 mK (cryogenic temperature). A qubit is implemented using a device called a transmon [28], which consists of an open-ended stub that acts as a capacitor and a Josephson junction (JJ) that acts as a nonlinear inductance. The JJ was modeled in a simulator with the inductance and port impedance connected in parallel. In addition, to obtain a

IEEE Transactions on Quantum Engineering

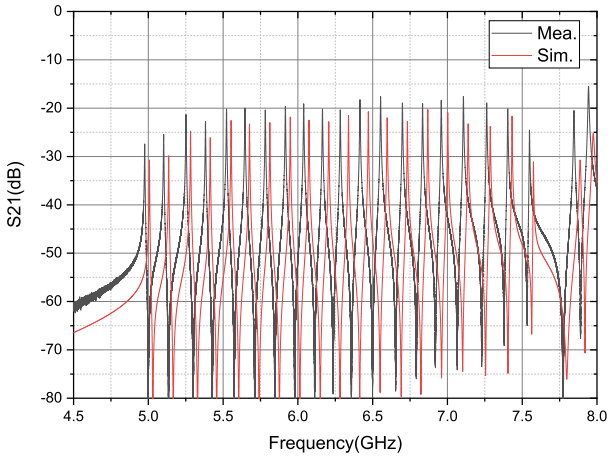

FIGURE 14. Simulated and measured transmission coefficient of the flute-shaped proposed multimode cavity resonator.

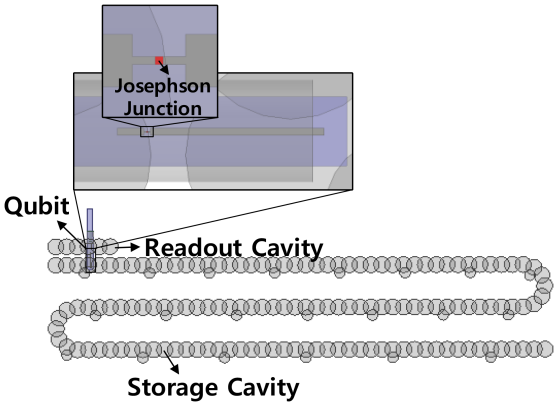

FIGURE 15. Quantum memory with maximized modes using proposed specific mode manipulated multimode storage cavity.

high quality factor, a transmon was fabricated on a sapphire substrate ($\varepsilon_r = 10$) with high purity.

It is important to design the components of a QM so that the mode is generated at the desired frequency, and that the photon can be stored/removed in the desired mode through transmon-cavity coupling.

Fig. 16 shows the simulated imaginary admittance (Y_{11}) obtained from the qubit for the proposed QMs. The qubit is embedded in the cavity and operates at a cryogenic temperature (~10 mK), and the qubit cannot be connected to any port that can be measured; therefore, the only option for verifying the overall QM is simulation. The resonant frequencies were obtained from the admittance plot, where the imaginary impedance was zero. In the case without an iris, the gap between the readout frequency and the 21st resonance frequency of the storage resonator or the 20th resonance frequency of the storage resonator is half the gap between the first and second resonance frequency. This means that the spacing of all resonance modes for QMs is not equal and that there is room for improvement in utilizing the given bandwidth. However, in the presence of an iris, the resonance

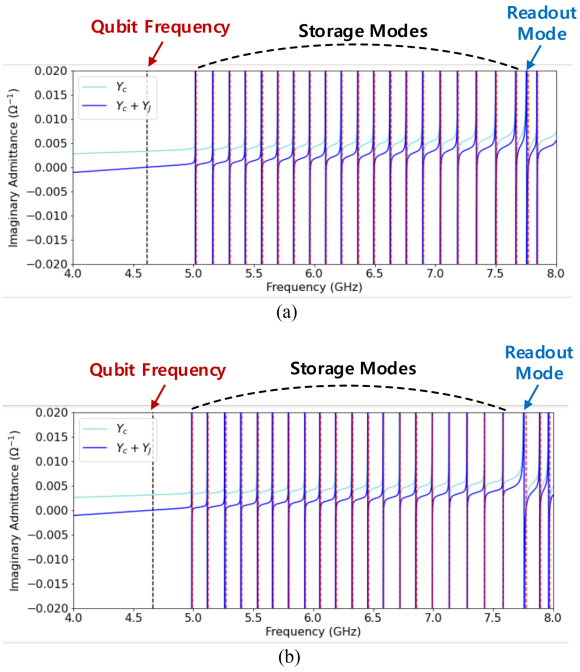

FIGURE 16. Simulated imaginary admittance (Y_{11}) seen from the qubit for the proposed quantum memories. (a) Without irises. (b) With irises.

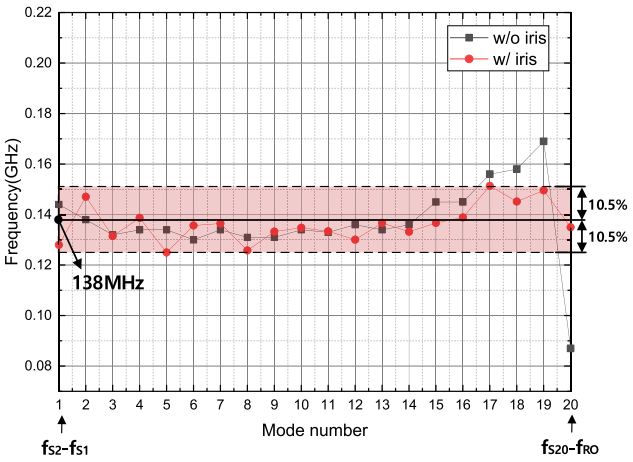

FIGURE 17. Simulated frequency spacing of the resonant frequencies of the quantum memories for with and without iris.

modes of all components are placed with equal spacing such that a mode-maximized design for QMs is possible.

Fig. 17 shows the simulated frequency spacing of the resonant frequencies of the QMs for cases with and without an iris. Compared with the case without an iris, it is clearly shown that the frequency spacing of the resonant frequency of the QM is in the range of 0.125–0.1514 GHz. The average spacing was 0.138 GHz and the distribution of the spacing was within 10.5% of the average. Fig. 18 shows the simulated g and χ values for the first 20 modes of the multimode storage cavity. The g and χ values were extracted from black-box superconducting circuit quantization, as described in [29]. In this case, the qubit frequency was set as 4.7193 GHz to obtain reasonable g and χ values. In the presence of irises,

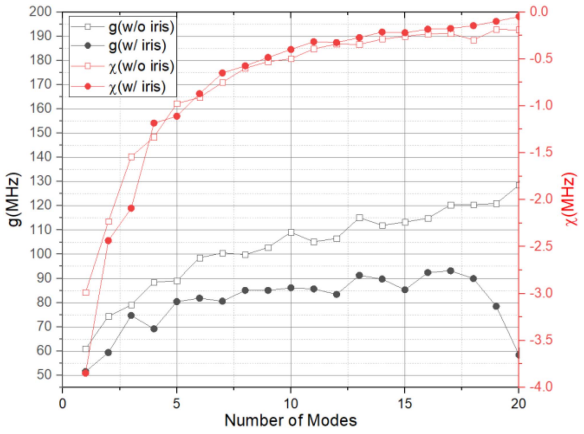

FIGURE 18. Simulated g and χ value for the first 20 modes and readout mode of the multimode storage cavity. The g and χ values were extracted from the black-box superconducting circuit quantization, which is described in [28].

compared with the case without irises, as the mode number increased, the absolute value of χ and the g value tended to decrease. This is because the higher the mode number, the greater is the effect of the irises. Nevertheless, it is predicted that quantum operation is possible because all the modes exist in the dispersive regime.

IV. CONCLUSION

A mode-manipulated multimode cavity QMs using several microwave techniques is proposed. First, by adjusting the geometry of the cavity to a quasi-elliptical shape, the overall interval characteristics could be adjusted to decrease monotonically, have equal intervals, or increase monotonically. Second, an iris structure was inserted into the multimode cavity to regulate a certain mode so that it was possible to insert the readout frequency to where the mode was originally placed.

The proposed QM devices were designed for the 5–8 GHz frequency band. The average spacing was 0.138 GHz and the distribution of the spacing was within 10.5% of the average. By demonstrating a mode-manipulated multimode cavity, it was possible to improve the performance of the QM by controlling the desired mode.

REFERENCES

[1] IEEE Spectrum, "Q&A with post-quantum computing cryptography researcher Jintai Ding," *IEEE Spectr.*, Nov. 2008. [Online]. Available: https://spectrum.ieee.org/qa-with-postquantum-computing-cryptography-researcher-jintai-ding

[2] M. Schuld and F. Petruccione, "Supervised learning with quantum computers," in *Quantum Science and Technology*. Berlin, Germany: Springer, 2018, doi: 10.1007/978-3-319-96424-9.

[3] Y. Cao et al., "Quantum chemistry in the age of quantum computing," *Chem. Rev.*, vol. 119, no. 19, pp. 10856–10915, 2019, doi: 10.1021/acs.chemrev.8b00803.

[4] L. K. Grover, "A fast quantum mechanical algorithm for database search," in *Proc. 28th Annu. ACM Symp. Theory Comput.*, 2019, pp. 212–219, doi: 10.1145/237814.237866.

[5] F. Arute et al., "Quantum supremacy using a programmable superconducting processor," *Nature*, vol. 574, pp. 505–510, 2019, doi: 10.1038/s41586-019-1666-5.

[6] S. Kwon, A. Tomonaga, G. L. Bhai, S. Devitt, and J.-S. Tsai, "Gate-based superconducting quantum computing," *J. Appl. Phys.*, vol. 129, 2019, Art. no. 041102, doi: 10.1063/5.0029735.

[7] J. C. Bardin, D. Sank, O. Naaman, and E. Jeffrey, "Quantum computing: Introduction for RF engineer," *IEEE Microw. Mag.*, vol. 21, no. 8, pp. 24–44, Aug. 2021, doi: 10.1109/MMM.2020.2993475.

[8] P. Krantz, M. Kjaergaard, F. Yan, T. P. Orlando, S. Gustavsson, and W. D. Olivar, "A quantum engineer's guide to superconducting qubits," *Appl. Phys. Rev.*, vol. 6, 2019, Art. no. 021318, doi: 10.1063/1.5089550.

[9] J. Kelly et al., "State preservation by repetitive error detection in a superconducting quantum circuit," *Nature*, vol. 519, pp. 66–69, 2015, doi: 10.1038/nature14270.

[10] R. K. Naik et al., "Random access quantum information processors using multimode circuit quantum electrodynamics," *Nature Commun.*, vol. 8, 2017, Art. no. 1904, doi: 10.1038/s41467-017-02046-6.

[11] C. Axline et al., "An architecture for integrating planar and 3D cQED devices," *Appl. Phys. Lett.*, vol. 109, 2016, Art. no. 042601, doi: 10.1063/1.4959241.

[12] T. Noh, G. Park, S. Lee, W. Song, and Y. Chong, "Construction of Controlled-NOT gate based on Microwave-activated phase(MAP) gate in two transmon system," *Sci. Rep.*, vol. 8, 2018, Art. no. 13598, doi: 10.1038/s41598-018-31896-3.

[13] E. Xie et al., "Compact 3D quantum memory," *Appl. Phys. Lett.*, vol. 112, 2018, Art. no. 202601, doi: 10.1063/1.5029514.

[14] M. Reagor et al., "Quantum memory with millisecond coherence in circuit QED," *Phys. Rev. B*, vol. 94, 2016, Art. no. 014506, doi: 10.1103/PhysRevB.94.014506.

[15] D. I. Schuster et al., "Sideband transitions and two-tone spectroscopy of a superconducting qubit strongly coupled to an on-chip cavity," *Phys. Rev. Lett.*, vol. 99, 2007, Art. no. 050501, doi: 10.1103/PhysRevLett.99.050501.

[16] P. J. Leek et al., "Using sideband transitions for two-qubit operations in superconducting circuits," *Phys. Rev. B*, vol. 79, 2009, Art. no. 180511, doi: 10.1103/PhysRevB.79.180511.

[17] R. W. Heeres et al., "Cavity state manipulation using photon-number selective phase gates," *Phys. Rev. Lett.*, vol. 115, 2015, Art. no. 137002, doi: 10.1103/PhysRevLett.115.137002.

[18] S. Chakram et al., "Multimode photon blockade," *Nature Phys.*, vol. 18, pp. 879–884, 2022, doi: 10.1038/s41567-022-01630-y.

[19] S. Chakram et al., "Seamless high-Q microwave cavities for multimode circuit QED," *Phys. Rev. Lett.*, vol. 127, 2021, Art. no. 107701, doi: 10.1103/PhysRevLett.127.107701.

[20] D. I. Schuster, R. K. Naik, and S. Chakram, "Technologies for long-lived 3D multimode microwave cvities," US Patent 20190288367, 2019. [Online]. Available: https://patentscope.wipo.int/search/en/detail.jsf?docId=US251642067

[21] D. Sun and J. Xu, "A novel iris waveguide bandpass filter using air gapped waveguide technology," *IEEE Microw. Wireless Compon. Lett.*, vol. 26, no. 7, pp. 475–477, Jul. 2016, doi: 10.1109/LMWC.2016.2574822.

[22] D. Oloumi, A. Kordzadeh, and A. A. Lotfi Neyestanak, "Size reduction and bandwidth enhancement of a waveguide bandpass filter using fractal-shaped irises," *IEEE Antennas Wireless Propag. Lett.*, vol. 8, pp. 1214–1217, 2009, doi: 10.1109/LAWP.2009.2035648.

[23] T. E. Rozzi, "Equivalent network for interacting thick inductive irises," *IEEE Trans. Microw. Theory Techn.*, vol. MTT-20, no. 5, pp. 323–330, May 1972, doi: 10.1109/TMTT.1972.1127752.

[24] T. S. Chen, "Characteristics of waveguide resonant irises filters," *IEEE Trans. Microw. Theory Techn.*, vol. MTT- 15, no. 4, pp. 260–262, Apr. 1967, doi: 10.1109/TMTT.1967.1126437.

[25] J. Schwinger and D. Saxon, *Discontinuities in Waveguides*. New York, NY, USA: Gordon and Breach, 1968.

[26] Y. Leviatan, P. G. Li, A. T. Adams, and J. Perini, "Single-post inductive obstacle in rectangular waveguide," *IEEE Trans. Microw. Theory Techn.*, vol. MTT-31, no. 10, pp. 806–812, Oct. 1983, doi: 10.1109/TMTT.1983.1131610.

[27] C. A. Balanis, "Ridgeted waveguide," in *Advanced Engineering Electromagnetics*. Hoboken, NJ, USA: Wiley, 1989, pp. 466–469.

[28] J. Koch et al., "Charge-insensitive qubit design derived from the cooper pair box," *Phys. Rev. A*, vol. 76, 2007, Art. no. 042319, doi: 10.1103/PhysRevA.76.042319.

[29] S. E. Nigg et al., "Black-box superconducting circuit quantization," *Phys. Rev. Lett.*, vol. 108, 2012, Art. no. 240502, doi: 10.1103/PhysRevLett.108.240502.